Stickiness effects in chaos

G. Contopoulos, M. Harsoula

Celest Mech Dyn Astr (2010) 107:77–92
DOI 10.1007/s10569-010-9282-6

ORIGINAL ARTICLE

Stickiness effects in chaos

G. Contopoulos · M. Harsoula

Received: 29 October 2009 / Revised: 21 April 2010 / Accepted: 21 April 2010 /
Published online: 18 May 2010

Abstract Stickiness is a temporary confinement of orbits in a particular region of the phase space before they diffuse to a larger region. In a system of 2-degrees of freedom there are two main types of stickiness (a) stickiness around an island of stability, which is surrounded by cantori with small holes, and (b) stickiness close to the unstable asymptotic curves of unstable periodic orbits, that extend to large distances in the chaotic sea. We consider various factors that affect the time scale of stickiness due to cantori. The overall stickiness (stickiness of the second type) is maximum near the unstable asymptotic curves. An important application of stickiness is in the outer spiral arms of strong-barred spiral galaxies. These spiral arms consist mainly of sticky chaotic orbits. Such orbits may escape to large distances, or to infinity, but because of stickiness they support the spiral arms for very long times.

Keywords Galactic models · Chaos · Stickiness · Barred spiral galaxies · Spiral arms

1 Introduction

Stickiness is the temporary concentration of chaotic orbits in particular regions of phase space. There are two types of stickiness: (a) stickiness around an island of stability (Fig. 1a) and (b) stickiness close to the unstable asymptotic curves of unstable periodic orbits that extend to large distances into the chaotic sea (Fig. 1b).

In the present paper we consider stickiness in 2-dimensional systems, namely in the standard map:

G. Contopoulos · M. Harsoula (✉)
Research Center for Astronomy, Academy of Athens, Soranou Efesiou 4, 11527 Athens, Greece
e-mail: mharsoul@academyofathens.gr

G. Contopoulos
e-mail: gcontop@academyofathens.gr

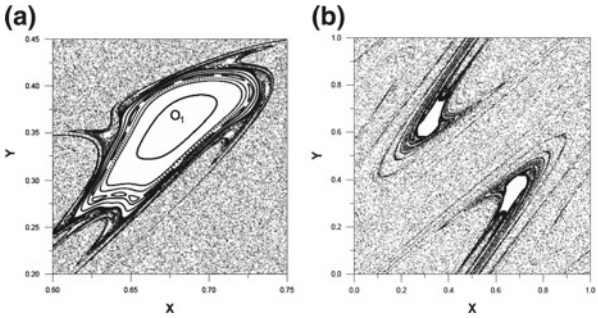

Fig. 1 Stickiness in the standard map for $k = 5$ **a** around an island of stability **b** close to the asymptotic curves in the chaotic sea

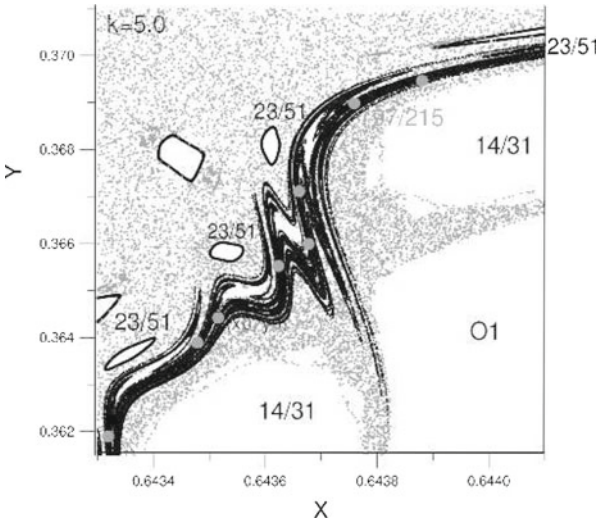

Fig. 2 An unstable asymptotic curve of the unstable periodic orbit 97/215 (with eigenvalue $\lambda = 254$) in the standard map for $k = 5$. We mark also some islands of stability and some chaotic regions inside and outside the cantorus $t_1 = [2, 4, 1, \ldots]$. On the $left$ and above the cantorus is the large chaotic sea

$$\begin{aligned} x' &= x + y' \\ &\quad (\mathrm{mod}1) \\ y' &= y + \frac{k}{2\pi}\sin(2\pi x) \end{aligned} \tag{1}$$

and in galactic models.

The first example of stickiness around two islands of stability was provided by Contopoulos (1971). After that time many people studied various aspects of stickiness (for a review and bibliography see Contopoulos and Harsoula 2010). In the present paper we summarize some of the most recent results.

The most important stickiness effects around an island of stability appear when the last KAM curve surrounding the island is destroyed, as the perturbation increases. Then a new last KAM curve is formed closer to the center of the island and the former last KAM curve becomes a cantorus with infinite holes. Orbits between this cantorus and the new last KAM curve stay for some time in this region, but they escape later into the outer chaotic sea.

In Fig. 2 we give an unstable asymptotic curve (for a definition see Contopoulos 2002) of the unstable periodic orbit with rotation number 97/215 for $k = 5$. This periodic orbit is inside the cantorus $t_1 = [2, 4, 1, \ldots]$. (The dots in $t_1 = [2, 4, 1, \ldots]$ represent an infinite sequence

of 1's). The expression $t = [a_1, a_2, a_3, \ldots]$ represents the rotation number of the cantorus, given in the form of a continuous fraction:

$$t = \frac{1}{a_1 + \frac{1}{a_2 + \frac{1}{a_3 + \cdots}}} \tag{2}$$

The number 97/215 is a truncation of the rotation number t_1, while 14/31, 23/51 are lower order truncations of t_1. The periodic orbits 97/215 and 14/31 are inside the cantorus, i.e. closer to the central island O_1, while the periodic orbit 23/51 is outside the cantorus. The asymptotic curve makes several oscillations back and forth outside the set of islands 14/31 that surround the main island O_1. We see at the top of Fig. 2 that the asymptotic curve 97/215 has crossed the cantorus t_1 because it has gone above the island 23/51 which is outside this cantorus.

In the present paper we study the main stickiness effects around islands of stability and along unstable asymptotic curves. In Sect. 2 we examine the various factors that affect the time scale of stickiness around an island of stability. In Sect. 3 we study the stickiness along the unstable asymptotic curves in the chaotic sea and we find how the two types of stickiness are related. Then in Sect. 4 we give an important application of stickiness in the case of barred spiral galaxies. Our main new results are summarized in Sect. 5 which contains our conclusions. Finally in the Appendix we study the limits of the various islands where most of the stickiness effects take place.

2 Time scale of stickiness

The best way to find the stickiness effects in detail is by calculating various asymptotic curves of unstable periodic orbits, close to the last KAM curve. These unstable asymptotic curves make in general several oscillations parallel to the boundary of the island, before escaping to the large chaotic sea further away from the island. In particular, the asymptotic curves from unstable periodic orbits inside a cantorus, pass through the holes of the cantorus outwards, but they return several times inside the cantorus before escaping far into the large chaotic sea. We define the escape time as the number of mappings needed by a chaotic orbit with initial conditions close to the periodic orbit to cross the $y = 0$ axis. There are several factors that affect the escape time from the neighborhood of an island, namely the sign and the magnitude of the eigenvalues of the periodic orbits, the size of the gaps of the main cantorus and the effects of other cantori, islands and asymptotic curves.

2.1 The sign and the magnitude of the eigenvalues

The eigenvalue of an unstable periodic orbit P with rotation number n/m is calculated after one mapping, i.e. after $2m$ iterations. From every point P_i of the orbit P start two unstable asymptotic curves at opposite directions (eigenvectors) and two stable asymptotic curves, again at opposite directions. The eigenvalues of the periodic orbit are inverse, λ and $1/\lambda$, where $|\lambda| > 1$. If the eigenvalue λ is negative, successive mappings of a point of an asymptotic curve are alternatively on the opposite directions of the asymptotic curves. On the other hand, if the eigenvalue λ is positive, the orbits of an unstable asymptotic curve have mappings only on the same asymptotic curve. Although the eigenvalue $\lambda > 0$ is unique the asymptotic curves of opposite directions, escape (i.e. their orbits escape) at different rates, i.e. the asymptotic curve in one direction (fast direction) escapes faster than the asymptotic

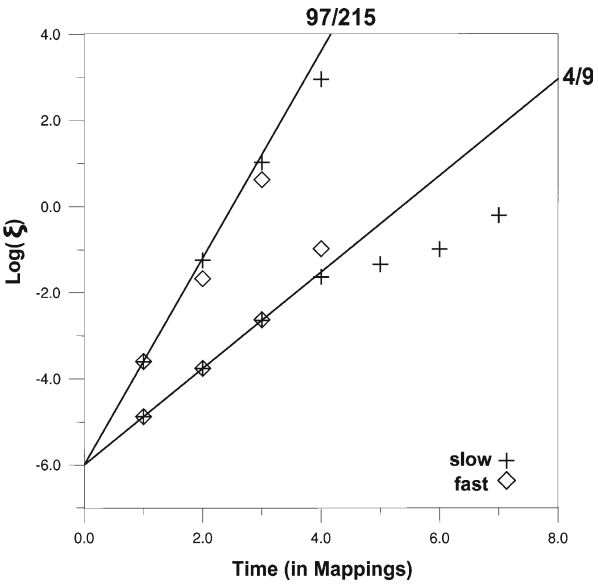

Fig. 3 The logarithm of the length ξ along the fast ($\diamond$) and slow (+) asymptotic curves from the orbits 97/215 and 4/9, starting at $\xi_0 = 10^{-6}$ as functions of time measured by the numbers of mappings until escape. We mark the values of $\log \xi$ at successive mappings up to the last mapping before escape. The *straight lines* represent the formula (3) (for $k = 5$)

curve of the other direction (slow direction). An example of the fast and slow direction of the asymptotic curves is shown in Fig. 3 of Contopoulos and Harsoula (2008).

In Fig. 3 we mark the escape times along the asymptotic curves from two periodic orbits for $k = 5$, and the length ξ of the asymptotic curves until their escape. According to the linear theory the length ξ is given by the formula $\xi = \xi_0 |\lambda|^T$, where ξ_0 is the initial deviation (in the present case $\xi_0 = 10^{-6}$) and T is the time, measured in mappings. Thus we have

$$\log \xi = \log \xi_0 + T \log |\lambda| \tag{3}$$

The inclinations of the straight lines (3) (Fig. 3) are equal to the logarithms of $|\lambda|$. Thus for larger $|\lambda|$ these lines are more steep. We see that the linear estimates are valid up to large distances although the lengths ξ are measured along curves with many oscillations back and forth. For longer times the values of ξ deviate from the linear theory, but the linear approximation gives the correct order of magnitude. In Fig. 3 we see also the difference between the fast ($\diamond$) and the slow (+) orbits. In some cases the length ξ is very large, because the asymptotic curve undergoes many oscillations, near the border of the island O_1 before escaping. E.g. in the case of the orbit 97/215 with $\lambda = 254$, ξ reaches the value of 10^3 before escaping.

2.2 Stickiness near a cantorus

The KAM curves are defined by their rotation number around the center of an island. If θ_i are the angles between the vectors joining the center of the island with the successive points along an invariant curve, the rotation number rot, or rotational frequency ν_θ, is the average value of θ_i (divided by 2π), after N iterations with N tending to infinity.

Another useful quantity is the twist number, or twist frequency ν_φ, which is the average of the angles φ_i (divided by 2π) between the deviation vectors from successive points. Along the invariant curves around the center of the island O_1 we have $\nu_\theta = \nu_\varphi$. However, along any

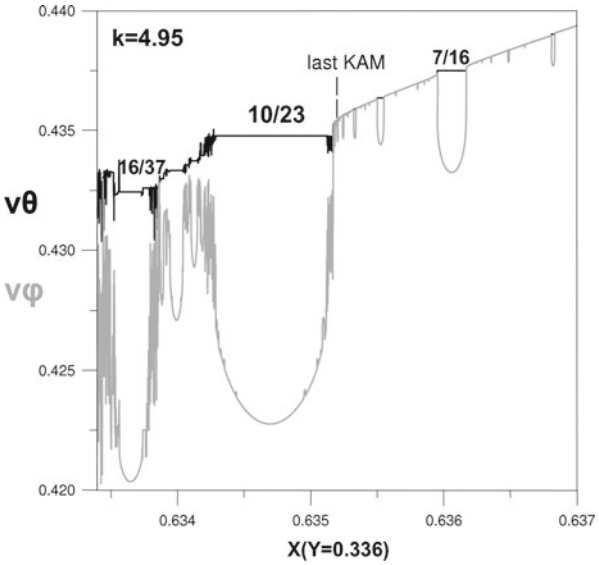

Fig. 4 The rotation number ν_θ, and the twist number ν_φ, as functions of x along a line $y = 0.336$ for $k = 4.95$. The two lines coincide for all rotation numbers that are not rational, up to the last KAM curve. At the rational numbers we have islands of stability with $\nu_\theta = \text{const.}$ while the curve ν_φ forms cups

secondary island around the original island the rotation number is constant, while the twist number varies. The difference $\nu_\theta - \nu_\varphi$ is called epicyclic frequency (Voglis et al. 1999).

In Fig. 4 we give the functions ν_θ and ν_φ calculated around O_1 for orbits starting along a particular line. This line ($y = 0.336$) intersects several secondary islands like 7/16 as we move to the left, outwards from the center of the island O_1. The functions ν_θ and ν_φ decrease outwards (to the left). The curves ν_θ and ν_φ are tangent all along the invariant curves, i.e. when ν_θ is not a rational number (resonance). However, at every resonance the curve ν_θ has a plateau, while the curve ν_φ forms a cup. The curve ν_θ is like a devil's staircase (Gutzwiller 1990) because it has plateaus at an infinite number of rational values, but changes at all irrational values. At the boundaries of the plateaus there are small chaotic regions, in which neither ν_θ nor ν_φ are accurately defined. On the other hand the curve ν_φ has infinite cups.

The two curves stop being tangent beyond the last KAM curve to the left (Fig. 4). However, there are also secondary islands in the chaotic region, and along these islands ν_θ is constant and ν_φ forms again a cup. This is the case of the resonances 10/23 and 16/37.

When the last KAM curve is destroyed by increasing the perturbation k, beyond a critical value k_c, it becomes a cantorus, i.e. a cantor set with an infinite number of holes (Aubry 1978; Percival 1979). Just before the destruction of the last KAM curve a chaotic layer is formed both inside and outside it. After its destruction the inner and the outer chaotic layers communicate. The combined chaotic layer extends inwards up to a new last KAM curve, which is closer to the center of the island O_1.

In Fig. 5 we give the curves ν_θ and ν_φ for $k = 4.9977$ and $k = 4.9978$ and we mark the most important islands and cantori by their rotation numbers. For $k = 4.9977$ the curves ν_θ and ν_φ are tangent along small intervals close to the tori $t_3 = [2, 4, 1, 1, 1, 1, 3, 1, \ldots]$ and $t_2 = [2, 4, 1, 1, 1, 1, 2, 1, \ldots]$ but for $k = 4.9978$ all the tori in the range of this figure have been destroyed. The most resistant torus in this region is t_2 because it exists also for $k = 4.99775$, when t_3 has been destroyed. The distance between a local maximum ν_φ from the curve ν_θ gives an estimate of the importance of a cantorus. When this distance is small the gaps of the cantorus are small (see Sect. 2.3). When k is just larger than k_c the holes of the cantorus are very small and the escape time is very large. Then the orbits inside the

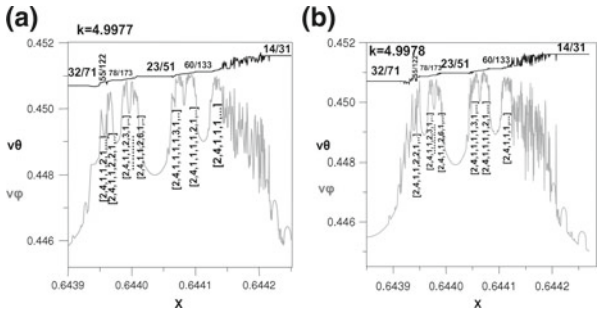

Fig. 5 The curves ν_θ and ν_φ for **a** $k = 4.9977$ and **b** $k = 4.9978$. We mark certain tori, cantori and islands by their rotation numbers

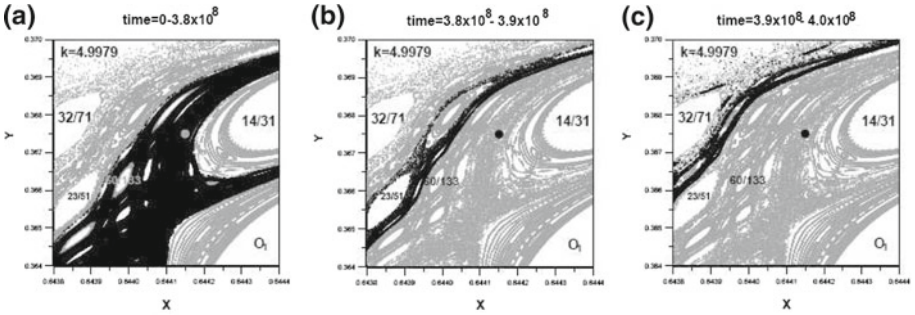

Fig. 6 **a** An orbit for $k = 4.9979$ starting at the dot ($x = 0.64415$, $y = 0.3675$) fills almost ergodically the chaotic domain inside the cantorus $t_2 = [2, 4, 1, 1, 1, 1, 2, 1, \ldots]$ (*black area*) up to $T = 3.8 \times 10^8$ iterations, then it diffuses outwards in the time intervals **b** $T \epsilon (3.8 \times 10^8 - 3.9 \times 10^8)$ and **c** $T \epsilon (3.9 \times 10^8 - 4.0 \times 10^8)$. In the last case most black points are in the chaotic sea on the *left* and above the limits of the figure

cantorus have sufficient time to cover ergodically the whole chaotic domain inside the cantorus. An example is given in Fig. 6a (for the standard map) where we see an orbit calculated for $t = 3.8 \times 10^8$ iterations that fills practically ergodically the chaotic region inside the cantorus $t_2 = [2, 4, 1, 1, 1, 1, 2, 1, \ldots]$ up to a new last KAM curve (around O_1) inside the set of islands 14/31 for $k = 4.9979$. However, after $t = 3.8 \times 10^8$ the asymptotic curve stays for some time around the islands 23/51 and then diffuses gradually outwards (Figs. 6b,c). Because of the approximate ergodicity of orbits inside the cantorus t_2 the escape times for orbits starting inside this cantorus are approximately the same, ranging between 10^8 and 10^{10} (Fig. 7). However, when the gaps of the cantorus become larger, the escape time decreases outwards. As we go out of the main cantorus (the cantorus with the smallest gaps) the escape time decreases exponentially. This is seen in Fig. 7 for $k = 4.9979$. The escape time is given along a line parallel to the y-axis. Close to the cantorus t_2 the decrease follows a law $\log T = -3231y + 1199$ (upper black line) with a large inclination (3231), but further out (near and to the left of the border of Fig. 7) it follows a law $\log T = -1434y + 538$ (lower black line) with a much smaller inclination (1434). These formulae give the average times of escape. However, near every island the escape times increase superexponentially (Morbidelli and Giorgilli 1995) and tend to infinity as we approach the border of the island from outside.

2.3 The sizes of the gaps

The escape time through a cantorus depends mainly on the sizes of the gaps. If the gaps are small the escape time is very large and tends to infinity as the size of the gaps tends to zero.

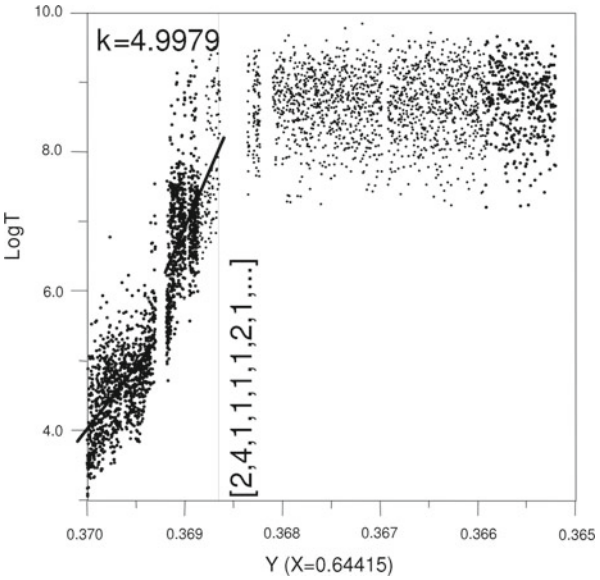

Fig. 7 The escape time T as a function of y along the line $x = 0.64415$ of Fig. 6a for $k = 4.9979$. The time T is roughly constant inside the cantorus [1,4,1,1,1,1,2,1,…] except at the small islands in this region where it is infinite. Outside this cantorus the escape time decreases exponentially

The calculation of the gaps in a cantorus is described in Contopoulos and Harsoula (2010). An approximate formula relating the escape time T to the maximum gap of the cantorus $t_2 = [2, 4, 1, 1, 1, 1, 2, 1, \ldots]$ (Fig. 8a) is

$$\log T = A + \frac{B}{\mathrm{Max}G} \tag{4}$$

with $A = 1.30$ and $B = 0.033$.

A better approximation is given by the minimum distance of the curves ν_θ and ν_φ near a cantorus. When all invariant curves are destroyed in a certain domain the curves ν_θ and ν_φ are no more tangent (Fig. 5b) and the minimum distance $|\nu_\theta - \nu_\varphi|$ corresponds to the cantorus with the smallest gaps.

An approximate formula relating the escape time T with the minimum distance $|\nu_\theta - \nu_\varphi|$ at the cantorus t_2 (Fig. 8b) is:

$$T = \frac{C}{\mathrm{Min}|\nu_\theta - \nu_\varphi|^2} \tag{5}$$

with $C = 0.25$. The quantity $\mathrm{Min}|\nu_\theta - \nu_\varphi|$ is more easily calculated than $\mathrm{Max}G$.

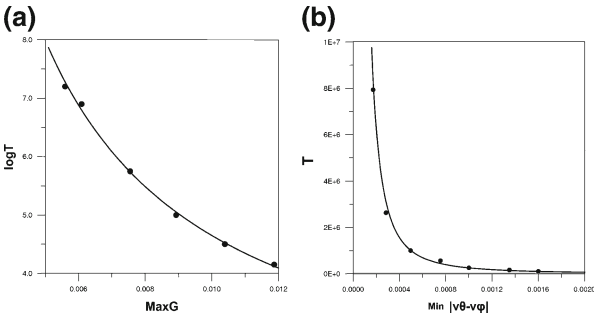

Fig. 8 **a** The logarithm of the escape time T as a function of the maximum gap of a cantorus Max G. **b** The escape time T as a function of $\mathrm{Min}|\nu_\theta - \nu_\varphi|$

2.4 Other cantori, islands and asymptotic curves

When an orbit or an unstable asymptotic curve passes through a cantorus it does not escape fast into the large chaotic sea, because there are further obstructions due to other cantori, islands and unstable asymptotic curves of other periodic orbits. E.g. an orbit in Fig. 5b from the neighborhood of the island 14/31 passes through the cantorus t_1, but then it has to pass through the cantori t_2 and t_3 before reaching the neighborhood of the island 23/51. Then it has still to pass the cantori [2,4,1,1,2,3,1,…] and [2,4,1,1,2,2,1,…] before coming close to the island 32/71. On the left of the resonance 32/71 there are no more important cantori to be crossed until the orbit reaches the outer chaotic sea. Of course the most important barrier is the cantorus which has the smallest gaps. But as the orbit approaches the other cantori it remains close to them for some time before proceeding further (Fig. 6b,c).

Furthermore an orbit has to avoid the higher order islands that appear in most places of phase space (see Figs. 2 and 6). In fact near every last KAM curve there are stable and unstable periodic orbits corresponding to the successive truncations of the rotation number (2) like $rot_1 = \frac{1}{a_1}, rot_2 = \frac{1}{a_1+\frac{1}{a_2}}$ etc. However, after a last KAM curve becomes a cantorus all stable periodic orbits close to it become unstable. As the perturbation increases the region inside and outside the cantorus that does not contain islands becomes larger (Contopoulos et al. 1987).

But even if all the stable periodic orbits close to a given cantorus have become unstable, the unstable asymptotic curves of the various unstable periodic orbits provide a partial barrier. In fact the unstable asymptotic curves cannot cross themselves, or each other. Thus all unstable asymptotic curves proceed in an almost parallel way and take a long time until they reach the outer chaotic sea.

3 Stickiness along unstable asymptotic curves

The unstable asymptotic curves of the orbit O (0,5,0) surround the islands O_1, O_1', but they extend also to large distances in the chaotic sea, outside the islands. Thus the stickiness close to these unstable asymptotic curves supports the sticky regions around the islands O_1, O_1', but generates also dark lines far from these islands.

A similar behavior is expressed by the unstable asymptotic curves of the periodic orbits close and around the border of the island O_1, e.g. the orbit 4/9. After these curves cross the most important cantori around this island, they extend to large distances in the chaotic sea, and as they cannot cross the unstable asymptotic curves of the orbit O (0.5,0.0) they are almost parallel to them. Thus the stickiness close to these unstable curves is almost the same as the stickiness close to the unstable curves of the orbit O.

Similar results are found if we take a set of nonasymptotic orbits starting in small domains of the space outside the various islands. In Fig. 1b we give a set of iterates of many non asymptotic orbits starting outside the island O_1. This should be compared with the form of the asymptotic curves U from the unstable periodic orbit O (Fig. 9a), and the asymptotic curve $U+$ from the unstable orbit 4/9 (Fig. 9b). It is remarkable that the sticky regions of Fig. 1b are very close to the asymptotic curves U and $U+$, which in turn are very close to each other. The asymptotic curves that extend to the large chaotic sea return again an infinite number of times close to the boundary of the island O_1, contributing to the stickiness around this island. Thus the stickiness along the asymptotic curves far from the island is intimately connected with the stickiness around the island O_1 (and the island O_1').

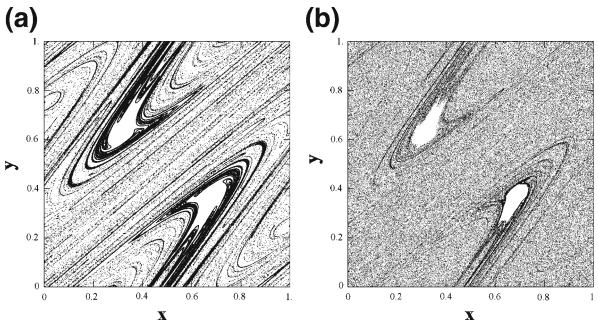

Fig. 9 The unstable asymptotic curves **a** U from the orbit O (0.5, 0.0) (25 iterates of 2×10^4 initial points in an interval 10^{-6} from O) **b** $U+$ (slow asymptotic curve) from the point P_1 of the orbit 4/9 (15 iterates of 2×10^4 initial points in an interval 10^{-6} from P_1)

Orbits starting close to an island of stability remain close to it, exhibiting stickiness due to the existence of cantori outside the last KAM curve surrounding the island, until they escape to the large chaotic sea. The "escape time" is called also "initial stickiness time". However, the orbits escaping for the first time from the neighborhood of an island into the large chaotic sea return later an infinite number of times close to the island O_1, contributing again to the stickiness around this island and the maxima of the overall density of points after some time are near the unstable asymptotic manifolds (see Fig. 10a of Contopoulos and Harsoula 2008).

The stickiness near the unstable asymptotic curves is a very natural phenomenon. In fact orbits close to an unstable periodic orbit approach this orbit along directions almost parallel to the stable asymptotic curves, but after they come close to the unstable orbit they deviate along a direction almost parallel to the unstable asymptotic curve. This behavior explains the appearance of dark lines in the distribution of the iterates of the sets of initial conditions in phase space (Fig. 1b). However, after a long time, the density of points outside the islands becomes uniform. This phenomenon was discussed also by Sun et al. (2005), who emphasized the role of the hyperbolic sets for stickiness.

In general if a periodic orbit is close but outside an island, its unstable asymptotic curves return close to the island many times after exiting into the chaotic sea, contributing again to the stickiness around the island. However, after a sufficiently long time the density of points near and far from the island tends to become equal (Contopoulos and Harsoula 2008).

4 Applications in barred spiral galaxies

It is well known that the spiral arms of galaxies are density waves (Lin and Shu 1964) i.e. they are not composed always of the same stars, but the stars pass through them, staying there for relatively long times. Thus the density maxima are along the spiral arms. In the normal spirals the perturbations are weak, of the order of 2–10% of the axisymmetric background, and the orbits are mostly ordered with relatively small deviations from circular (Lin and Shu 1964; Contopoulos 2002). In such cases chaos is insignificant. But in barred spiral galaxies the perturbations due to the bar are of order 50–100%, and chaos is quite important.

In strong barred spiral galaxies we see an important application of the phenomenon of stickiness of chaotic orbits. Using a galactic model of an N-body simulation we study the role of sticky chaotic orbits in supporting the spiral arms for times comparable to the age of the Universe (the Hubble time). More precisely, we use a galactic model called "QR4" which is one out of four N-body experiments in Voglis et al. (2006) simulating barred spiral

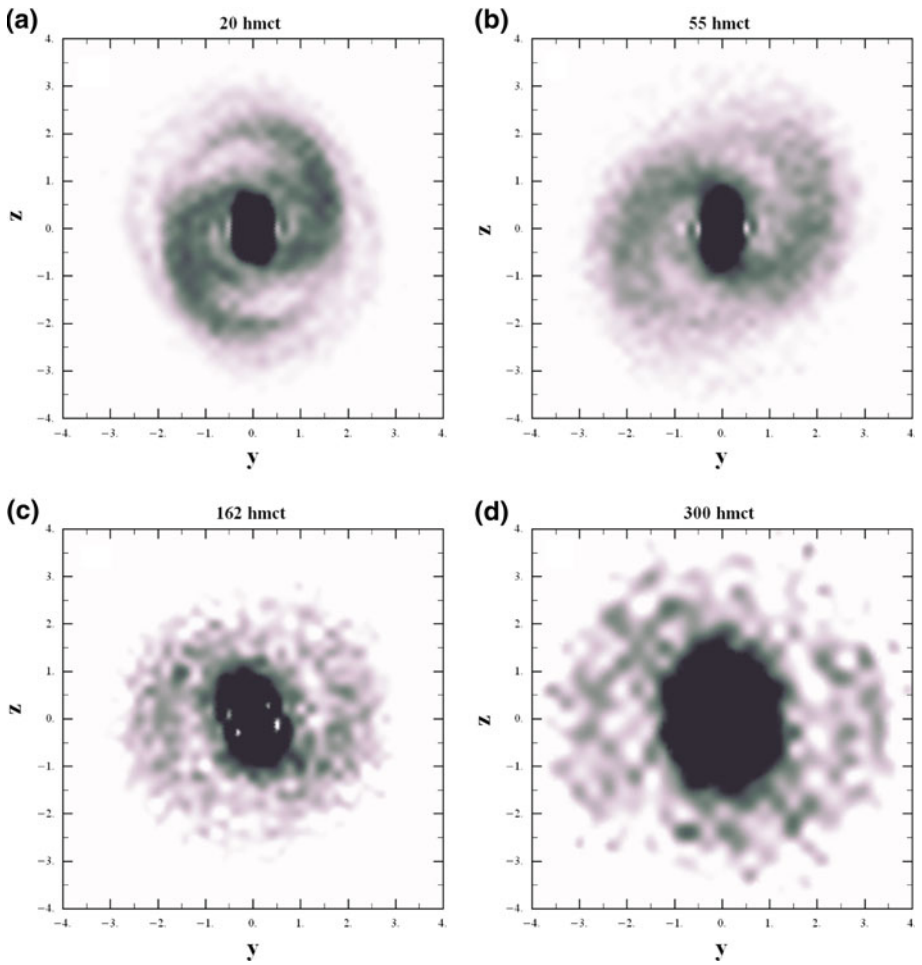

Fig. 10 The projection on the plane of rotation of our *N*-body model after various times **a** 20 *hmct* **b** 55 *hmct* **c** 162 *hmct* and **d** 300 *hmct* (corresponding approximately to a Hubble time)

galaxies with different pattern speed velocities. Details for the initial conditions of the experiment "QR4" can be found in Voglis et al. (2006). In that paper the authors have studied the percentages of chaotic orbits during the time evolution of these experiments towards a temporary equilibrium state. In Fig. 10 we plot the projection of the experiment "QR4" on the $y-z$ plane (the plane of rotation), for four different snapshots during their time evolution, namely for 20 half mass crossing times of the system (hereafter $hmct$) in Fig. 10a, 55 *hmct* in Fig. 10b, 162 *hmct* in Fig. 10c and 300 *hmct* in Fig. 10d (which corresponds approximately to 1 Hubble time). Spiral arms are visible approximately up to 0.5 Hubble time, while a significant $m=2$ spiral mode still exists even for a Hubble time.

In order to explain this relatively robust shape of spiral arms we isolate a snapshot corresponding to 55 *hmct* (Fig. 10b). By using a frozen potential that corresponds to this time, we study the role of chaotic and regular orbits separately in supporting the shape of the galaxy. The following discussion corresponds to this specific snapshot. Figure 11 shows the

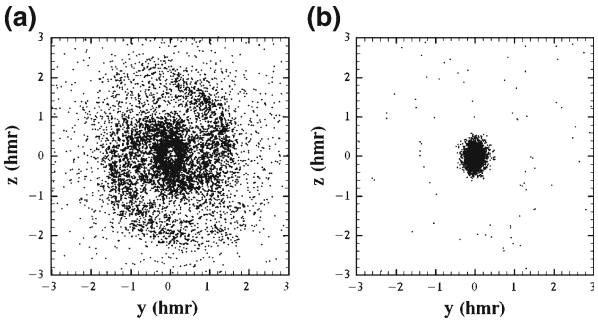

Fig. 11 **a** The chaotic orbits are along the spiral arms and the envelope of the bar **b** The ordered orbits are mainly in the main body of the bar. Units are in half mass radius of the system (hmr)

projection of the chaotic particles (Fig. 11a) and of the ordered particles (Fig. 11b) separately, on the plane of rotation. From this figure it is obvious that chaotic orbits populate the spiral arms beyond the ends of the bar, and the envelope of the bar, while the ordered orbits form the main body of the bar (Fig. 11b) (Voglis et al. 2006). The orbits in the main body of the bar are quite elongated and not close to circular, but nevertheless they are ordered. On the other hand the orbits beyond the ends of the bar are quite irregular, but they support the spiral arms for very long times. These orbits may go to large distances from the galaxy and eventually they may acquire positive energy and escape to infinity along hyperbolic like orbits (Contopoulos and Patsis 2006). However, for quite long times the orbits remain close to the main body of the galaxy and populate preferably the spiral arms beyond the ends of the bar even if some orbits finally escape. The reason for this behavior is that these orbits are sticky along and close to the asymptotic curves of the unstable asymptotic curves of the main unstable periodic orbits near corotation (Tsoutsis et al. 2009).

In Fig. 12a we give the distribution of the radial velocities (on the plane of rotation) of the N-body particles of our galactic model. It is obvious that the maximum of the distribution is around the zero value, i.e. most of the particles are located close to the apocenters or the pericenters of their orbits. The same distribution is valid for every snapshot during the evolution of the N-body simulation. This means that the orbits spend statistically more time at their apocenters-pericenters modulating the shape of the galaxy through density waves. Another important result is the distribution of the Jacobi constants (E_j) of all the orbits. The Jacobi constant is given by the relation:

$$E_j = \frac{1}{2}(v_x^2 + v_y^2 + v_z^2) + V(x, y, z) - \frac{1}{2}\Omega_p^2(y^2 + z^2) \tag{6}$$

where v_x, v_y, v_z are the velocities in the rotating frame of reference, $V(x, y, z)$ is the potential in the position (x, y, z), and Ω_p is the pattern speed velocity of the bar.

In Fig. 12b we give the distribution of the Jacobi constants for all the orbits (dashed line), for the regular orbits (gray line) and for the chaotic ones (black line). We observe that the maximum for the total distribution lies at the same value of E_j as the maximum of the distribution of the chaotic orbits. The corresponding value of E_j is close to the Jacobi constants of the Langrangian points L_1, L_2 along the bar. At this energy level there are almost only chaotic orbits. These orbits play an important role in supporting the spiral arms of the galaxy in the sense that most of them stay located for a long time close to the asymptotic curves (on the phase space) of the most important unstable periodic orbits that exist around corotation and outside it.

An example of an important unstable periodic orbit near the ends of the bar is the orbits PL_1 and PL_2 around the Lagrangian points L_1 and L_2 respectively, at corotation. In fact

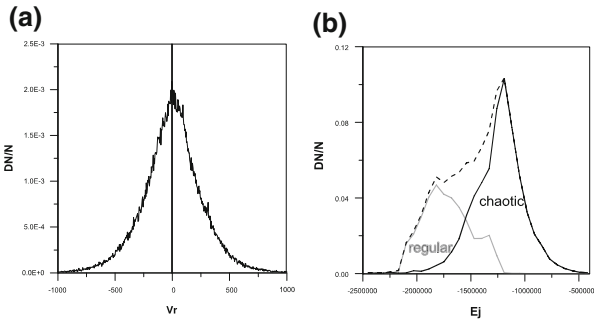

Fig. 12 **a** The distribution of the radial velocities of the real N-body particles on the $y-z$ plane (plane of rotation) **b** The distribution of the Jacobi constants (E_j) for the regular orbits (*gray line*), for the chaotic orbits (*black line*) and for all the N-body orbits (*dashed line*). The maximum of the distribution corresponds to a value close to $E_j(L_1)$, $E_j(L_2)$, where only chaotic orbits exist

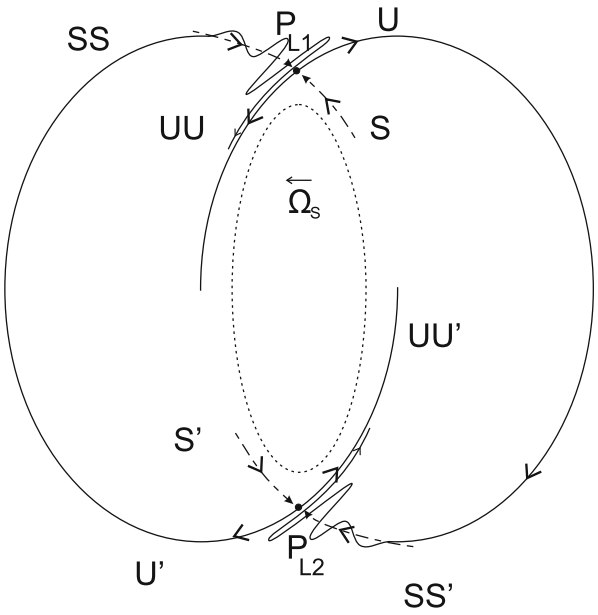

Fig. 13 The unstable periodic orbits PL_1, PL_2 around the Lagrangian points L_1, L_2 at the end of the bar for a particular value of the Jacobi constant, and their asymptotic manifolds (schematic)

the main body of the bar terminates near corotation (Contopoulos 1980; Sanders and Tubbs 1980; Schwarz 1984; Elmegreen and Elmegreen 1985; Kent 1990; Sellwood and Wilkinson 1993). The orbits PL_1, PL_2 are nearly elliptical. Their asymptotic manifolds intersect the configuration plane along two unstable and two stable asymptotic curves (Fig. 13) defined by the apocenters or the pericenters of the orbits. Two unstable manifolds (U, U') form spiral structures extending to large distances from the ends of the bar. The other unstable manifolds (UU, UU') are close but outside the main body of the bar.

Orbits in the neighborhood L_1 or L_2 approach the unstable periodic orbits along paths close to S, SS and S', SS' and then they deviate either along and close to the outer unstable asymptotic curves U, U', which are trailing, or close to the inner asymptotic curves UU, UU', in the envelope of the bar, which are leading (Fig. 13 gives a schematic representation).

The individual orbits reach the asymptotic curves at their apocenters or pericenters (having zero radial velocity, $v_r = 0$) and they stay there for relativity long times, before they come again closer to the bar. Thus the apocenters and pericenters ($v_r = 0$) are the maxima of the density.

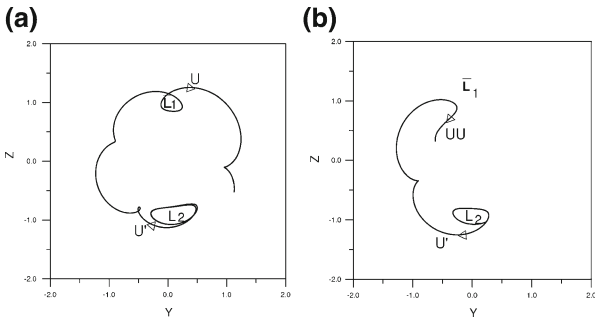

Fig. 14 Orbits starting close to the short period orbit PL_2 around L_2 approach the Lagrangian point L_1 and then deviate **a** along U, or **b** along UU

The spiral asymptotic curve U' further away from L_2 approaches the point L_1 and then makes larger and larger oscillations close to the asymptotic curves U and UU from L_1 (Fig. 13). Thus it brings material close to L_1, that is supporting the spiral U from L_1 and the envelope of the bar along UU. Furthermore the material that goes close to U and UU comes again close to L_2 and replenishes the material that goes close to the spiral U' from PL_2. Figure 14 presents two real chaotic N-body orbits in the area of corotation, both starting close to the unstable PL_2 orbit. In Fig. 14a the orbit following the U' asymptotic direction reaches the area of L_1 and then deviates near the spiral, along the U asymptotic direction, while in Fig. 14b the orbit when reaching the area of L_1 deviates near the UU asymptotic direction close to the envelope of the bar.

Besides the orbits PL_1PL_2 there are several other unstable periodic orbits in the broad neighborhood of corotation whose asymptotic curves are forced to be parallel to the ones of PL_1 and PL_2 as they are not allowed to intersect each other. Even at energy levels where the PL_1 and PL_2 orbits do not exist there are other unstable periodic families that trap the chaotic orbits around their asymptotic curves and reinforce the structure of the spiral arms. The orbital analysis of all the ordered and chaotic orbits of our N-body model is presented in Harsoula and Kalapotharakos (2009) for two different snapshots of the galaxy evolution. We have found that several chaotic orbits are close to the resonances 4/1 inside corotation and to $-4/1$, $-2/1$ and $-1/1$ outside corotation. Furthermore there are periodic orbits PL_4 and PL_5 close to the Lagrangian points L_4, L_5 which are unstable for a large range of Jacobi constants and their unstable asymptotic curves also support the spiral arms.

An example of how the manifolds of the apocenters and the pericenters of several unstable periodic orbits can construct the shape of the spiral arms is given in Fig. 15. In Fig. 15a we plot the projection of the N-body particles on the plane of rotation when integrated until their radial velocities become for the first time zero ($v_r = 0$). Therefore, all the particles of Fig. 15a lie at the apocenters or the pericenters of their orbits. If we compare this figure with Fig. 10b we see that the spiral arms are better outlined when all the particles lie exactly at their apocenters or pericenters. In Fig. 15b we plot the 2-D approximation of the asymptotic curves of the apocenters and pericenters of two families, namely the PL_1, PL_2 unstable periodic orbits at a Jacobi constant that corresponds to the maximum of the energy distribution (Fig. 12b). We notice that the shapes of these manifolds coincides with the shapes of the spiral arms. The integration of the manifolds has been done in a frozen potential for a total time that corresponds to approximately 0.5 Hubble time.

If we integrate the orbits along the unstable asymptotic curves for longer time, they may go to large distances from the galaxy, and as there exist no closed invariant curves surrounding the galaxy (in the phase space) they can escape to infinity. However, the real N-body chaotic orbits are sticky close to these asymptotic curves in the phase space, and therefore close to

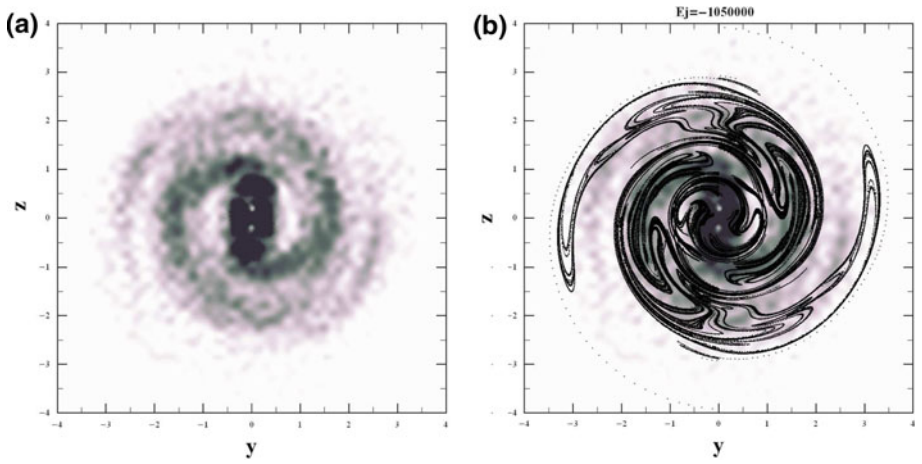

Fig. 15 **a** The projection of the N-body particles on the plane of rotation when integrated until their radial velocities become exactly zero ($v_r = 0$) for the first time, i.e. we plot all the particles when they reach the apocenters or the pericenters of their orbits. **b** The projection of the manifolds of the apocenters and pericenters of the unstable periodic orbits PL_1, PL_2 on the configuration space, at a Jacobi constant E_j that corresponds to the maximum of the energy distribution (see Fig. 12b)

the spiral arms on the configuration space and they can preserve the shape of the spiral arms for times of the order of one Hubble time.

In Fig. 16 we plot the number of particles that escape beyond a radius of 4 *hmr* (that sets an approximate limit to the bounded part of the galaxy) as a function of time. It is obvious from this figure that there is an almost constant rate of escaping particles up to a certain time (of the order of 0.5 Hubble time), while this rate tends to decrease after longer times. The escaping orbits after a Hubble time (≈300 *hmct*) amount to about 20% of the chaotic orbits. Therefore, it is obvious that chaotic orbits support the spiral arms of the galaxy for a long time, due to the phenomenon of stickiness, but after a much longer time they may escape to infinity.

5 Conclusions

The main new results of this paper are:

(1) The time scale of stickiness around an island of stability depends on the following factors (a) the sign and magnitude of the eigenvalues of the unstable periodic orbits in the sticky zone. (b) the sizes of the gaps of the main cantorus and (c) the barriers produced by other cantori, islands and asymptotic curves.
(2) The logarithm of the length ($\log \xi$) along an unstable asymptotic curve is given approximately as a linear function of the time, despite the fact that the asymptotic curves make many oscillations, until this curve reaches the chaotic sea.
(3) If the gaps of a cantorus are small the orbits inside the cantorus cover a chaotic region for a long time almost ergodically. After crossing this cantorus the orbits are still confined for some time by other cantori, before escaping to the chaotic sea.
(4) The logarithm of the escape time ($\log\ T$) is given approximately as a linear function of the inverse of the maximum gap. A better approximate formula gives the time T as proportional to the inverse of the square of the minimum distance $\mathrm{Min}|\nu_\theta - \nu_\varphi|$

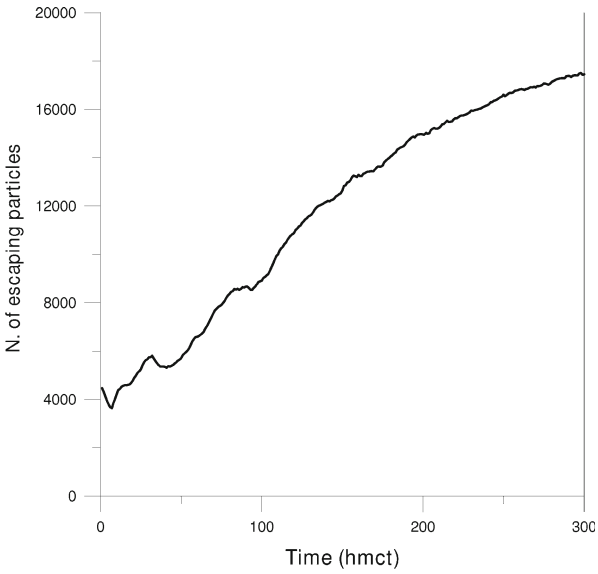

Fig. 16 The number of escaping particles beyond 4*hmr* as a function of time in *hmct* of the system

between the curves giving the rotation number (ν_θ) and the twist number (ν_φ) close to the cantorus.

(5) The stickiness along the unstable asymptotic curves is produced by orbits approaching these asymptotic curves over large distances in the chaotic sea. The nonasymptotic orbits approach the periodic orbits along curves almost parallel to stable asymptotic curves and then escape close to the unstable asymptotic curves. If a periodic orbit is around an island its unstable asymptotic curves return close to the island many times after exiting into the chaotic sea and they contribute again to the stickiness around the island for a long time. Thus the two types of stickiness are connected. After a longer time the density of points near and far from the island tends to become equal.

(6) An important application of the stickiness effects is in the structure of the spiral arms of strong barred spiral galaxies. In such cases the spirals are composed mainly of chaotic orbits. The stars along these chaotic orbits stay for a long time close to the unstable asymptotic curves of the main unstable periodic orbits and their apocenters and pericenters outline the shape of the spiral arms.

(7) The maxima of density of the chaotic orbits delineate the spiral arms outside the bar for long times, of the order of a Hubble time. After much longer times these orbits may escape altogether from the galaxy. Thus the persistence of the spiral arms is a stickiness effect.

References

Aubry, S.: In Solitons and Condensed Matter Physics. In: Bishop, A.R., Schneider, T. (eds.) Springer, New York 264 (1978)

Contopoulos, G.: Orbits in highly perturbed dynamical systems. III. Nonperiodic Orbits Astron. J. **76**, 147–156 (1971)

Contopoulos, G.: How far do bars extend, Astron. Astrophys. **81**, 198–209 (1980)

Contopoulos, G.: Order and Chaos in Dynamical Astronomy. Springer Verlag (2002), Second Printing (2004)

Contopoulos, G., Harsoula, M.: Stickiness in chaos. Int. J. Bifurcat. Chaos **18**, 2929–2949 (2008)

Contopoulos, G., Harsoula, M.: Stickiness effects in conservative systems. Int. J. Bif. Chaos (in press) (2010)
Contopoulos, G., Patsis, P.: Outer dynamics and escapes in barred galaxies. Mon. Not. R. Astron. Soc. **369**, 1039–1054 (2006)
Contopoulos, G., Varvoglis, H., Barbanis, B.: Large degree stochasticity in a galactic model. Astron. Astrophys. **172**, 55–66 (1987)
Elmegreen, E.G., Elmegreen, D.M.: Properties of barred spiral galaxies. Astrophys. J. **288**, 438–455 (1985)
Gutzwiller, M.C.: Chaos in Classical and Quantum Mechanics. Springer, New York (1990)
Harsoula, M., Kalapotharakos, C.: Orbital structure in N-body models of barred-spiral galaxies. Mon. Not. R. Astron. Soc. **394**, 1605–1619 (2009)
Kent, S.M.: The bar in NGC 4596. Astron. J. **100**, 377–386 (1990)
Lin, C.C., Shu, F.H.: On the spiral structure of disk galaxies. Astrophys. J. **140**, 646–655 (1964)
Morbidelli, A., Giorgilli, A.: Superexponential stability of KAM tori. J. Stat. Phys. **78**, 1607–1617 (1995)
Percival, I.C.: Nonlinear Dynamics and the Beam–Beam Interaction. In: Month, M., Herrera, J.C. (eds.) Amer. Inst. Physics, New York, 302 (1979)
Sanders, R.H., Tubbs, A.D.: Gas as a tracer of barred spiral dynamics. Astrophys. J. **235**, 803–820 (1980)
Sellwood, J.A., Wilkinson, A.: Dynamics of barred galaxies. Rep. Prog. Phys. **56**, 173–256 (1993)
Schwarz, M.P.: How bar strength and pattern speed affect galactic spiral structure. Mon. Not. R. Astron. Soc. **209**, 93–109 (1984)
Sun, V.S., Zhou, L.Y., Zhou, J.L.: The role of hyperbolic invariant sets in stickiness effects. Celest. Mech. Dyn. Astron. **92**, 257–272 (2005)
Tsoutsis, P., Kalapotharakos, C., Efthymiopoulos, C., Contopoulos, G.: Invariant manifolds and the response of spiral arms in barred galaxies. Astron. Astrophys. **495**, 743–758 (2009)
Voglis, N., Contopoulos, G., Efthymiopoulos, C.: Detection of ordered and chaotic motion using the dynamical spectra. Celest. Mech. Dyn. Astron. **73**, 211–220 (1999)
Voglis, N., Stavropoulos, I., Kalapotharakos, C.: Chaotic motion and spiral structure in self-consistent models of rotating galaxies. Mon. Not. R. Astron. Soc. **372**, 901–922 (2006)